Geophys. Astrophys. Fluid Dynamics, Vol. 89, pp. 169–203
Reprints available directly from the publisher
Photocopying permitted by license only

CONVECTIVE CIRCULATION IN MESOSCALE ABYSSAL BASINS

J. A. WHITEHEAD[a,*], G. K. KOROTAEV[b] and S. N. BULGAKOV[c]

[a] *Department of Physical Oceanography, MS-21, Woods Hole Oceanographic Institution, Woods Hole, Massachusetts 02543 USA;*
[b] *Department of Ocean Dynamics Processes, Marine Hydrophysical Institute, Sevastopol, 335000, Ukraine;*
[c] *Universidad de Guadalajara, Av. Vallarta 2602, sector Juares, C.P. 44100, Guadalajara, Jalisco, Mexico*

(Received 25 June 1996; In final form 4 July 1998)

Deep circulation in natural water basins that are smaller than the large global abyssal ocean, but bigger than a Rossby radius of deformation is both scantily documented and poorly understood. For buoyancy driving alone, angular momentum balance dictates that currents of both cyclonic and anticyclonic sense of circulation must exist, although both senses need not be of the same magnitude in the interior. Three laboratory experiments performed on a rotating turntable have been found with interior velocities that demonstrate layers with alternating cyclonic and anticyclonic azimuthal circulation. In one example an internal thermocline implies there is a set of two stacked meriodonal cells of opposite sign. Numerical results and laboratory data display qualitative agreement over a wide range of parameters. Quantitative comparison is within roughly two in the worst cases, but somewhat better for other cases. An argument based upon energetics is advanced which produces a velocity scale in rough agreement with some of the laboratory and numerical results.

Keywords: Circulation; mesoscale; convection

1. INTRODUCTION

The well known theory of deep ocean circulation by Stommel and Arons (1960) neglects surface wind stress effects on the ocean to a first

*Corresponding author. e-mail: jwhitehead@whoi.edu

approximation and focuses on buoyancy driven flows. The planetary beta-effect plays a crucial role in the formation of a balance between interior meridional flow and western boundary currents. Some quantitative assessment of the role of wind stress and buoyancy driving in establishing the vertical distribution of temperature has also been achieved. The theory has stimulated considerable oceanographic research (Warren, 1981).

Curiously, comparable studies of buoyantly driven circulation in mesoscale basins with the size range of 50–1000 km are less well developed. The understanding of dynamics within mesoscale basins is important not only for issues of biological and chemical health of the basins but also for an understanding of their response to forcing from the ocean's natural boundaries such as stress from the atmosphere, river runoff, and water flux from adjacent large basins. The small scale of a basin overrides the planetary beta effect producing other dynamical balances which must constrain the deep circulation.

Laboratory measurements and some associated numerical calculations are presented here of circulation in differentially heated axisymmetric cylinders as models of deep mesoscale basins. By "deep" we mean those driven only by buoyancy forces, with surface wind stress neglected. Two configurations of temperature distribution were used as models of deep mesoscale basins. The first one had high temperature imposed along the top and colder temperature imposed at the outer wall. The second one had hot temperature imposed along the top half of the sidewall and cold temperature along the bottom half.

Top priority was given to determining the flow patterns, circulation direction and to a lesser extent the temperature distribution. Stacked, axisymmetric, azimuthally circulating layers of alternating direction were always observed, and frequently three stacked layers with alternating circulation direction were measured for a wide range of parameters. Comparison of some of these with numerical calculations produced flow patterns very close to the experiments. In the experiment with differential sidewall temperature an internal thermocline was found. This requires two stacked meridional cells.

Quantitative measurement of the magnitude of azimuthal flow was taken whenever possible. There was not even a commonly accepted velocity or internal stratification scale for guidance, so the measurements were intended to give some data for the purpose of determining

such scales. A finite amplitude velocity scale for the motion is proposed, which is in crude agreement with measurements. Magnitudes of the measurements were not expected to precisely agree with the numerical results, which were actually conducted after the experiments were completed. Disagreement between the data and numerical calculations is in accord with estimated errors in the numerical integration from imperfect resolution of some of the boundary layers and imperfections in the experiment due to heat losses and finite conductivity of the glass walls.

To date, other studies have investigated some aspects of this type of problem, but none have looked at the whole problem we describe. Numerous studies focus on near-surface circulation in mesoscale basins. One motivation was that surface circulation in numerous lakes and inland seas has frequently been observed to be cyclonic. A number of mechanisms involving wind and thermal effects in concert with effects from fluid rotation have been proposed to produce this sense of circulation (Emery and Csanady, 1973; Wunsch, 1973; Bennett, 1975; Csanady, 1976, Csanady, 1977). Other studies focus on surface freshwater currents emanating into the ocean from local sources. These mimic the surface adjustment problem studied theoretically by Gill (1976). The freshwater currents which feed surface water into such basins deflect to the right in the Northern Hemisphere so that the freshwater density current leans against the right-hand wall and propagates in a cyclonic direction (Takano, 1955) with respect to the interior. This has been studied experimentally (Whitehead and Miller, 1979; Stern *et al.*, 1982; Griffiths and Hopfinger, 1983; Whitehead and Chapman, 1986; Griffiths, 1986), theoretically (Stern, 1980 as well as in some of the preceding papers), and numerically (Chao and Boicourt, 1986; Wang, 1987).

In contrast, study of the deep circulation is poorly understood compared to the understanding of the surface flows. Numerical models of the Black Sea circulation that reach to the full depth (Aubrey *et al.*, 1992; Oguz and Aubrey, 1995) possess anti-cyclonic gyres over the shelf break and cyclonic flow over the deep interior. Diagnostic calculations (Trukhchev and Demin, 1992) using a cross calibrated data set produce a horizontal component of circulation that appears more cyclonic near the bottom and anti-cyclonic at mid-depth. At this stage, direct observations of the circulation at great depth cannot

completely resolve such currents, but indications of flow in both cyclonic and anticyclonic directions are found by Bulgakov *et al.* (1994) and Bulgakov and Kushnir (1996). In contrast, vertical velocity and vertical mixing dominate the chemical transport within the deep waters and are key elements in producing the well known anaerobic conditions of the Black Sea. But what is the connection between lateral and vertical velocity?

In another example, the circulation of the Arctic basin is well known to be anti-cyclonic in the upper few hundred meters. In contrast, deeper flow appears to be cyclonic (Aagaard, 1981) although current meter or drifter data that illustrate the actual pattern of deep circulation in the Arctic ocean are absent. Detailed circulation patterns of the deep waters in other marginal seas such as the Caribbean, Indonesian, or Mediterranean seas are also only slightly documented at present. Circulation in the deepest and most remote small basins – deep ocean trenches – is virtually unknown, although there is some evidence of cyclonic recirculation over deep ocean trenches (Johnson, 1998).

The linearized theoretical limits previously used (Barcilon and Pedlosky, 1967a–c; Bulgakov and Korotaev, 1987; Bulgakov, 1987; Bulgakov *et al.*, 1992; Bulgakov *et al.*, 1996a; Pedlosky *et al.*, 1997) are exceeded by the experiments and numerical runs. Within the linearized context however, an appropriate dynamical balance for the flow is included in the analytical studies of linearly stratified fluid by Barcilon and Pedlosky (1967a–c). In these studies, the role of boundary layers and their contribution to circulation was studied in a rotating cylinder of stratified fluid. A recent comparison between laboratory measurements and calculations by Pedlosky *et al.* (1997) has resulted in a description of circulation driven by a differentially heated lid and its dependence upon dimensionless numbers expressing the relative role of stratification to rotation, friction to rotation, and friction to thermal diffusion. But in that problem the ambient stratification was specified. The flow pattern and temperature field was a small deviation from the resting rotating stratified state.

A variant of this problem, but without externally imposed stratification, was suggested by Bulgakov and Korotaev (1987) and Bulgakov (1987), who hypothesized that the circulation of the Black Sea is driven by a combination of river run-off and the intrusion of

salty water along different locations of the top outer radius. A simple theoretical model used temperature as a substitute for salinity. Flow was driven by variation of temperature on the sidewall; the top part was at a higher temperature than the bottom part. All other boundaries were insulated. Thermal conduction produces a region of warm water near the top sidewall and a region of cold water near the bottom sidewall with temperature extremes decaying away from that wall. The thermal wind relation from sidewall to offshore requires the fastest along-channel velocity at the top and bottom next to the wall. The flow direction corresponds to cyclonic direction of circulation in a cylindrical basin. At mid-depth the vertical shear is zero due to lack of lateral temperature change. But the net-drag in the along-channel direction must be zero since no external forces act in that direction. Since the top and bottom jets are in a direction corresponding to the cyclonic direction in a cylindrical basin, the zero shear region at mid-depth must correspond to a jet in the opposite (anticyclonic) direction. Although the governing equations were similar to those used by Barcilon and Pedlosky (1967) they were not linearized in a way that led to simple analysis over such a wide range of parameters.

Vorticity considerations such as those invoked by Monismith and Maxworthy (1989) also indicate the likelihood of such a flow pattern. Now consider flow in a cylinder of rotating fluid. Thermal conduction and viscous drag from heating of the top part of the sidewall must produce rising in a top sidewall thermal boundary layer. This requires a downward return flow near the middle. The latter produces vertical vortex stretching near the top interior. In contrast thermal conduction and viscous drag from cooling of the bottom part of the sidewall must produce descent in a bottom sidewall thermal boundary layer. This requires an upward return flow. This also produces vertical vortex stretching near the bottom interior. Thus the production of a cyclonic sense of circulation should be expected from vortex stretching in the interior of the cylinder near the top and bottom boundaries. In contrast, there will be vertical convergence at mid-depth in the interior of the channel. Vortex contraction will produce an anticyclonic sense of circulation there.

Force balances for steady flow along a channel, or angular momentum considerations for azimuthal forces in a cylinder, indicate the need for two flow directions in general. Take the azimuthal

momentum equation for the flow in cylindrical coordinates (integration in the angular direction is denoted by curly brackets):

$$\frac{\partial\{v\}}{\partial t}+\frac{\partial}{\partial r}\{uv\}+\frac{\partial}{\partial z}\{wv\}+\frac{\{uv\}}{r}+f\{u\}=\nu\left(\nabla^2\{v\}-\frac{\{v\}}{r^2}\right). \quad (1)$$

If multiplied by radius r this becomes an equation for angular velocity, which is equivalent to angular momentum in the Boussinesq approximation. Integrated over volume this becomes the angular momentum integral,

$$\int_0^D\int_0^R r^2\frac{\partial\{v\}}{\partial t}\,dr\,dz+\int_0^D r^2\{uv\}\Big|_{r=0}^{r=R}dz+\int_0^R r^2\{uw\}\Big|_{z=0}^{z=D}dr$$
$$+\int_0^R fr^2\left(\int_0^D\{u\}dz\right)dr$$
$$=\frac{\mu}{\rho}\left(\int_0^D\left[r^2\frac{\partial\{v\}}{\partial r}-r\{v\}\right]_{r=0}^{r=R}dz+\int_0^R r^2\frac{\partial\{v\}}{\partial z}\Big|_{z=0}^{z=D}dr\right). \quad (2)$$

The terms on the left-hand side contain the change of angular momentum plus the effect of pumping angular momentum in and out of the boundaries of the container. All these are zero for steady flow in closed containers with fixed boundaries. The left-hand side is also zero for steady flow in which fluid with the same angular momentum is pumped in and out. Assuming the left-hand side to be zero and rearranging slightly, we obtain

$$\int_0^D r\frac{\partial}{\partial r}(r\{v\})\Big|_{r=0}^{r=R}dz+\int_0^R r^2\frac{\partial\{v\}}{\partial z}\Big|_{z=0}^{z=D}dr=0 \quad (3)$$

so that total torque from boundary stress is zero. The above holds for axisymmetric containers of any shape. Boundary stress by a viscous boundary layer has a drag component pointed in a direction opposite to the interior velocity. Thus azimuthal circulation must be cyclonic in some regions and anti-cyclonic in others.

Salinity driven laboratory experiments (Fig. 1) displayed such layered cyclonic and anticyclonic circulation patterns (Bulgakov *et al.*, 1996b).

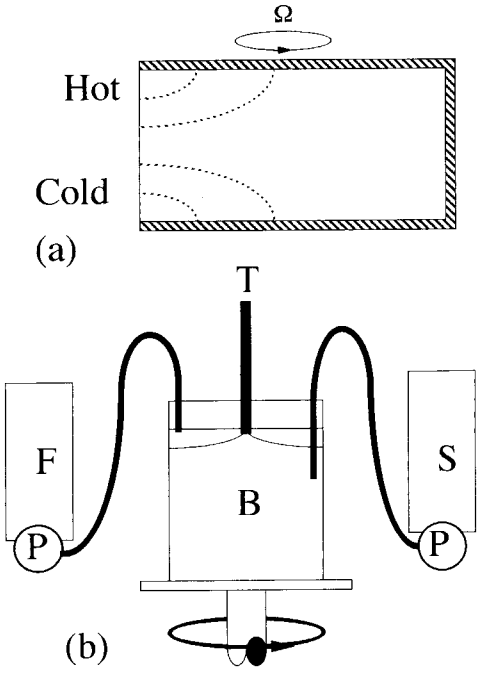

FIGURE 1 (a) The conceptual model of Bulgakov and Korotaev (1987). A vertical temperature distribution on the sidewall of a rotating insulated channel produces a temperature distribution as shown by the isotherms (dotted curves). The consequent density distribution in conjunction with thermal wind produces maximum positive velocities at the top and bottom with a minimum in between. (b) The experimental apparatus with salinity driving. B denotes the experimental basin, F the fresh water tank, S the salt water tank, P two pumps, and T the tube pipe which is connected to a spillway for removing water. The curves indicate the rough shape of the interface between salty and fresh water.

The experiments contained a constant flux source of freshwater at the surface and salty water at depth placed along the outer radius of a rotating cylindrical container of water. In order to maintain constant fluid depth, water was withdrawn at the top center. This resulted in (3) not being strictly satisfied. In spite of this, for most experiments a three layer structure of currents was found with cyclonic circulation at the top and bottom and anti-cyclonic circulation in the middle, as illustrated by the evolution of initially vertical dye streaks in Figure 2. But quantitative comparison between experiment and theory was not reported.

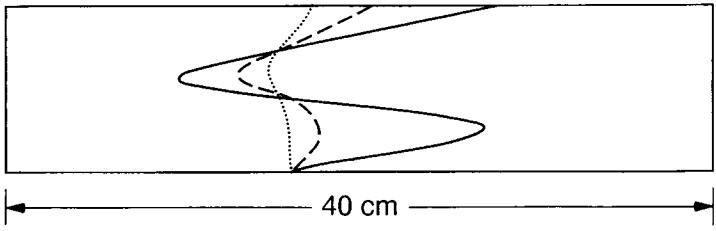

FIGURE 2 An initially vertical dye line at three times in a salt driven experiment. Time sequence is dot-dash-solid. The line is swept to the right (cyclonic direction) near the top and bottom and to the left at middle depth. The intensity of the surface circulation was about 0.4 cm/s.

2. THERMOCLINE DRIVEN TEMPERATURE EXPERIMENTS

We begin with a simple and common configuration for oceans or lakes with warm temperature imposed at the surface and cold temperature imposed along the side (Fig. 3a). The interior circulation in Figure 3a

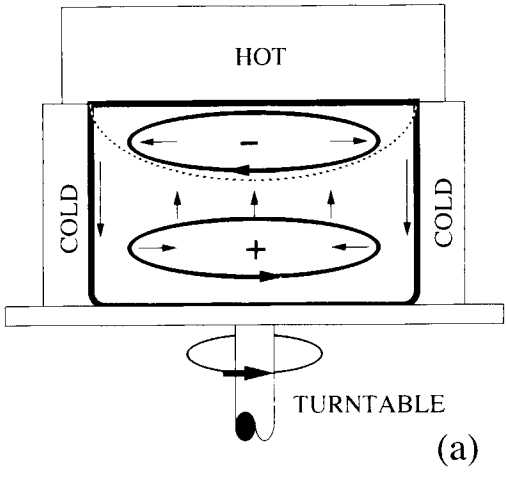

FIGURE 3 (a) Sketch of the first laboratory configuration with high constant temperature imposed on the top lid and lower temperature imposed on the sidewalls. The dotted curve indicates an isotherm. Meridional flow is indicated by straight arrows. Vertical vorticity is increased by stretching or decreased by contraction. The sign of vorticity is encircled by ellipses which show the sense of circulation compared to the ellipse showing the turntable's rotation. (b) Sketch of the second configuration. A rotating cylinder is given different sidewall temperature above and below the midplane. Symbols as in (a).

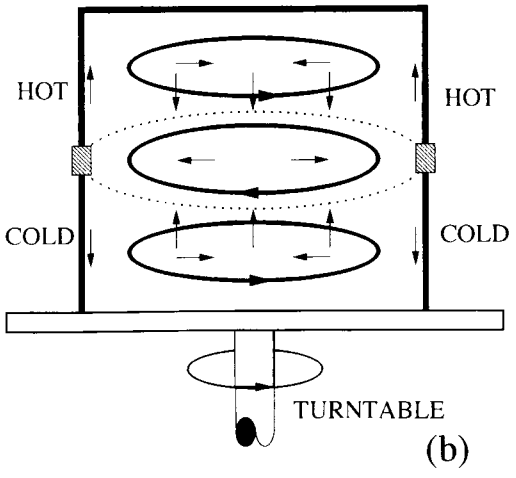

FIGURE 3 (Continued).

is sketched to resemble the lower half of the circulation in Figure 3b which is the configuration of the second set of experiments. This similarity masks an important difference between the two. There is a rigid boundary on the top of Figure 3a rather than a second body of fluid above the mid-plane.

Eleven experiments were conducted in an apparatus resembling the configurations in Figure 3a. A common laboratory beaker of 15.3 cm diameter and test fluid depth of 5 cm was filled with thymol blue and placed in a cold constant temperature bath. The beaker's bottom contained a layer of solid paraffin roughly 1 cm thick which provided both flatness and thermal insulation. A slightly smaller beaker was fitted into the top portion of this beaker by being placed onto a horizontal rubber gasket cemented to the wall 5 cm above the paraffin bottom. The smaller beaker was filled with circulating water from another thermostatic bath which was warmer than the first bath by an amount ΔT. Beakers and baths were all located on a uniformly rotating turntable.

To visualize flow the thymol blue technique was used. This was superior to the dye injection used in the exploratory salinity driven experiments and is suitable for quantifying very slow flows. Thymol blue solution, a pH sensitive indicator, was buffered to the yellow side

of its transition pH. When 1.5 volts was applied between two electrodes in the fluid, the solute around one (active) electrode changed to a dark blue with little change in fluid density. In our case, the active vertical brass electrode was placed in the field of view approximately 0.65 cm distance from the outer wall of the test tank and the passive electrode was out of sight. Flow was indicated by lateral movement of the dye away from the vertical wire after the electrode is activated. A photograph of dye distorted in this way is shown in Figure 4a and 25 seconds later in Figure 4b. Cells in the dye obviously come from double diffusion and produce complications in the dye pattern, but in general lateral displacement was greater than vertical displacement from these effects. Many images for data analysis were taken at earlier times when dye was less distorted and at reduced voltages so that in typical cases cells from double diffusion of the dye were smaller than in the photograph. Fronts of the dyed jets were easily measured to < 1 mm. The lateral displacements of velocity

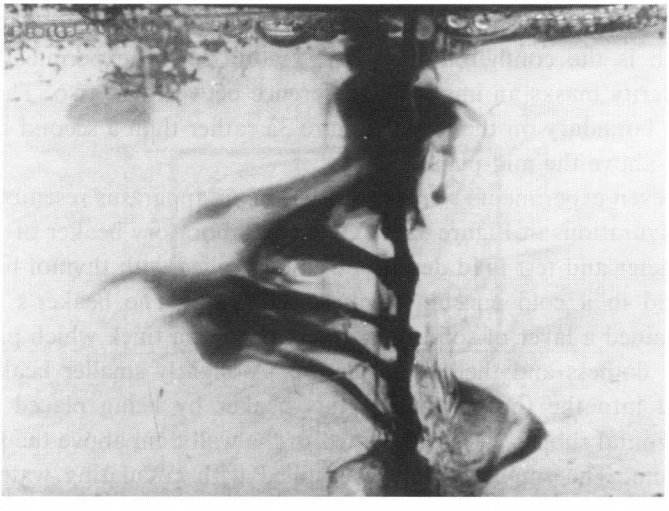

(a)

FIGURE 4 (a) Photograph of vertical dye streaks after they have been swept sideways by the flow. The cellular nature of the dye pattern is probably due to double diffusive effects and irregularities in the dye from small hydrogen bubbles on the electrode. Electrode voltage was made high to produce dark dye for this photograph. Such irregular cells are less pronounced at lower voltages and earlier times. (b) The same streaks about 25 seconds later. The dye has been swept laterally and the displacement reveals the three layers of azimuthal circulation. (c) Typical trajectory of sideways displacement of three maxima of the dye streak. Velocity data were found by taking a least squares fit line as shown.

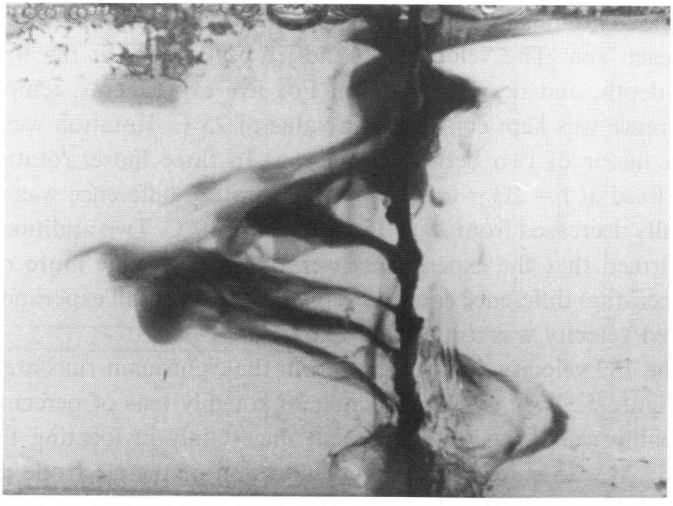

(b)

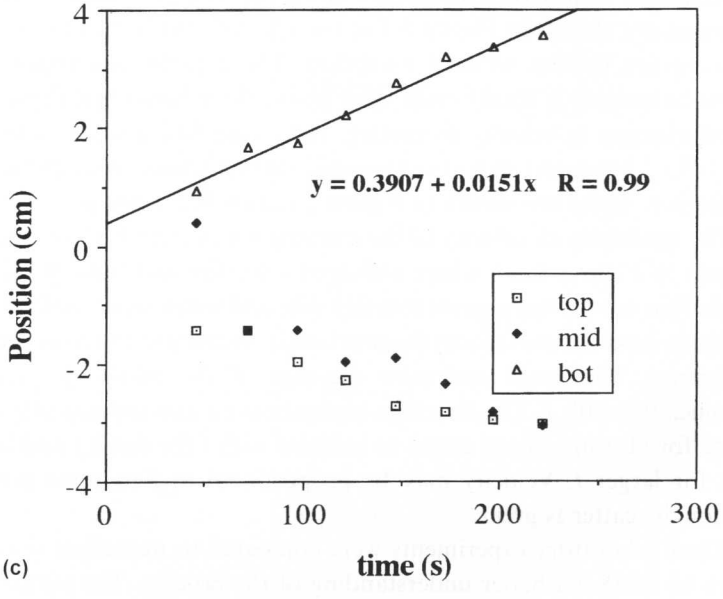

(c)

FIGURE 4 (Continued).

extrema were measured at a number of times and the trajectories fit by least squares. Examples are shown in Figure 4c. Speeds below 0.1 mm/s existed.

Velocity data were gathered over a period of more than four hours for each run. The velocities at the jet peaks were at the top, near mid-depth, and near the bottom. For five experiments, temperature difference was kept constant at a value of 25°C. Rotation was varied by a factor of two between each run. In three more, rotation rate was fixed at $f = 2\Omega = 0.5\,s^{-1}$ and temperature difference was systematically decreased from 20 to 15 and then to 10°C. Two additional runs confirmed that the experiments were repeatable. One more run had temperature difference equal to zero to serve as a null experiment, and indeed velocity was too slow to detect.

The 189 velocity mesurements from the eight main runs are shown in Figure 5. They exhibited scatter of roughly tens of percent which probably was due to measurement uncertainly in locating the edge of the dye. In some video frames, location of the electrode position was obscured by the dye, and this also contributed to error. The experiments with fixed temperature difference of 25°C and decreasing rotation are shown in Figure 5 frames a, b, c, d and h. Both signs of velocity are present without exception. The experiments appear to come to roughly a steady state after about three hours but there are small changes in velocity thereafter. Four runs had a fixed value of $f = 0.5\,s^{-1}$ but each run had successively smaller values of temperature difference. These are shown in Figure 5 frames b, e, f and g.

The sensitivity of velocity to the external parameters is shown more clearly in Figures 6a, b where averaged velocities and their standard deviations are plotted against rotation rate and temperature difference. In these experiments velocity is surprisingly insensitive to temperature difference. The speed and even the sign of the middle jet varies significantly with f. The direction of the bottom and top jets stay the same for all runs. Speed seems to increase with f for small f and level out for larger f. Velocity may be proportional to f to some power although scatter is great.

These laboratory experiments were compared to numerical simulations to achieve a better understanding of the process. The numerical study considered an axially symmetric motion of rotating fluid in a cylinder of depth H spinning with rate Ω. The above laboratary parameters ($H = 5\,cm$ and radius $R = 15.3/2\,cm$) were used to enable comparison between the laboratory and numerical results. A temperature difference ΔT was applied between the top surface and outer

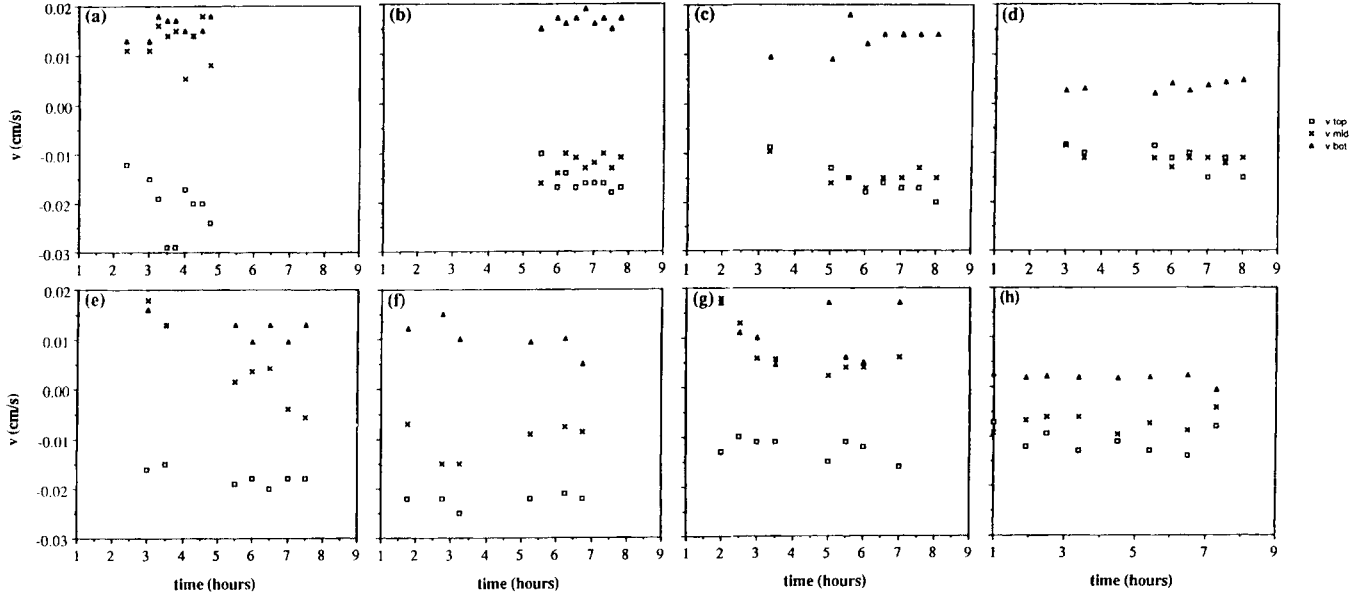

FIGURE 5 Velocity measurements for eight runs for the experimental configuration shown in Figure 3a. In (a)–(d) and (h) temperature difference ΔT was 25°C and f took the values 1.0, 0.5, 0.25, 0.125, and 0.063 s^{-1} respectively. In (b) and (e)–(g), f was 0.5 s^{-1} and temperature difference was 25, 20, 15, and 10°C respectively.

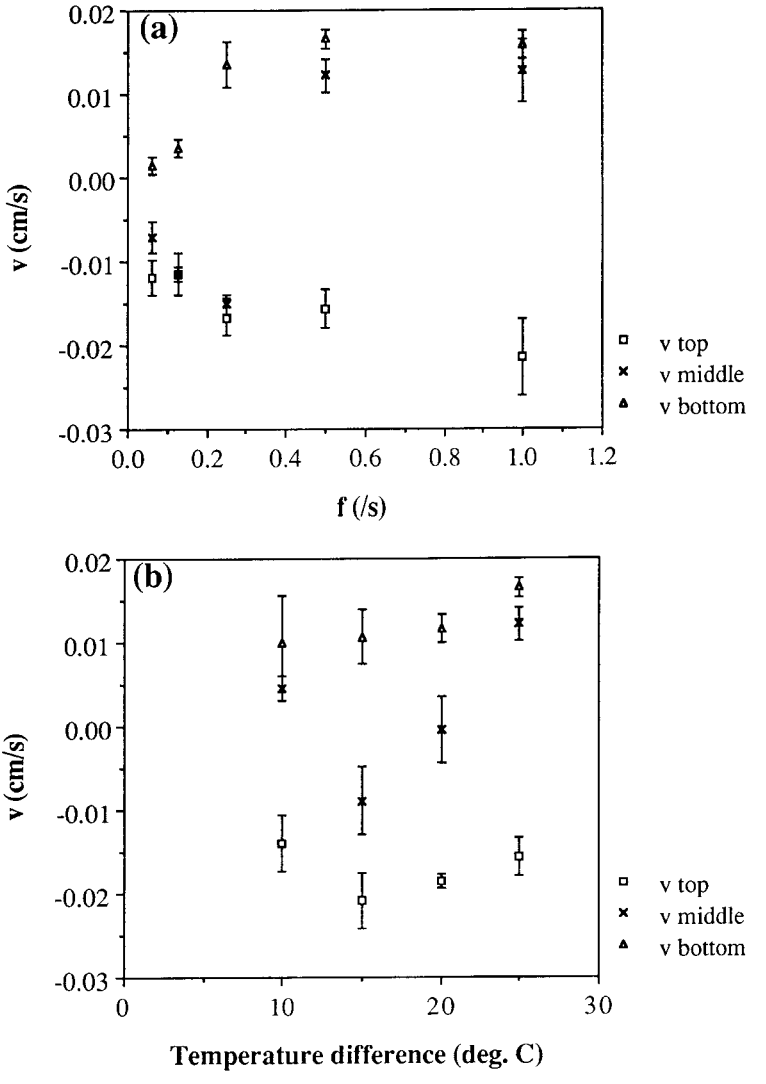

FIGURE 6 Averaged velocity data from the data shown in Figure 5. (a) Experiments with fixed temperature difference and different values of f as shown in Figures 5a–d and h. (b) Experiments with fixed rotation rate and different values of ΔT as shown in Figures 5b, f, g and h.

wall to produce conditions comparable to the laboratory experiments. The incompressible, hydrostatic Boussinesq approximations were used. A linear equation of state relating temperature and density is

used with constant coefficient of expansion α. This was set equal to its approximate value at 20°C of $2 \times 10^{-4}\,°\mathrm{C}^{-1}$.

Laboratory experiments show that the Rossby number u/fL is at most 0.1. This is based on the greatest azimuthal velocity magnitude of about 0.03 cm/s in Figure 5, using the smallest rotation rate of $f = 0.063\,\mathrm{s}^{-1}$ with a geometric length scale of $L = 5\,\mathrm{cm}$. Linear momentum equations are appropriate for such small Rossby number. A few runs whose results are not shown confirmed that acceleration or centrifugal terms were smaller than the Coriolis force. The following Boussinesq equations were used for the numerical simulations:

$$\frac{\partial u}{\partial t} - fv = -\frac{1}{\rho}\frac{\partial p}{\partial r} + \nu\left(\nabla^2 u - \frac{u}{r^2}\right), \tag{4a}$$

$$\frac{\partial v}{\partial t} + fu = \nu\left(\nabla^2 v - \frac{v}{r^2}\right), \tag{4b}$$

$$0 = -\frac{1}{\rho}\frac{\partial p}{\partial z} + g\alpha T, \tag{4c}$$

$$\frac{\partial T}{\partial t} + u\frac{\partial T}{\partial r} + w\frac{\partial T}{\partial z} = \kappa\nabla^2 T, \tag{4d}$$

$$\frac{1}{r}\frac{\partial}{\partial r}(ru) + \frac{\partial w}{\partial z} = 0, \tag{4e}$$

where

$$\nabla^2 = \frac{1}{r}\frac{\partial}{\partial r}\left(r\frac{\partial}{\partial r}\right) + \frac{\partial^2}{\partial z^2}.$$

Here, z is the vertical coordinate, r is the radial coordinate, radial velocity is u, azimuthal velocity is v, vertical velocity is w, pressure is p and temperature is T. Viscosity and thermal diffusion coefficients are equal to those of water, that is $\nu = 0.01\,\mathrm{cm}^2\,\mathrm{s}^{-1}$ and $\kappa = 0.0014\,\mathrm{cm}^2\,\mathrm{s}^{-1}$, reduced gravity is $g\alpha T$. These are almost identical to the equations with Rossby number and stratification zero as derived in Pedlosky *et al.* (1997) although they are in dimensional form. The two

differences are (a) that the nonlinear terms in the heat equation are retained since no other term can balance thermal conduction even though they too were shown to be scaled by Rossby number, and (b) the hydrostatic approximation was used in (4c). Boundary conditions were

$$u = v = w = 0 \text{ and } T = \Delta T \quad \text{at} \quad z = 0, \tag{5}$$

$$u = v = w = \frac{\partial T}{\partial z} = 0 \quad \text{at} \quad z = H, \tag{6}$$

$$u = v = \frac{\partial T}{\partial r} = 0 \quad \text{at} \quad r = 0, \tag{7}$$

$$u = v = w = T = 0 \quad \text{at} \quad r = R, \tag{8}$$

where H is the depth of the basin and R is its radius.

Figure 7 shows the results of numerical calculations after the numerical equivalent of eight laboratory hours for distribution of azimuthal velocity, the meridional streamfunction, and temperature for $\Delta T = 25°\text{C}$ and for two different values of rotation $f = 0.5$ and $0.063\,\text{s}^{-1}$ respectively. Anti-cyclonic circulation occupies a region close to the top. Flow with cyclonic sense appears throughout the rest of the region. The meridional circulation consists of a large cell with upwelling in most of the basin and downwelling near the wall. Outward radial velocity is found in a top boundary region and in a region above the bottom. Inward flow is found in a region below the top boundary and in a bottom boundary region. The strength of vertical velocity is independent of the vertical coordinate in the bottom portion of the interior as in the Pedlosky *et al.* (1997) solution for small S. This is less true in the top region. Temperature exhibits isotherms which are almost horizontal throughout much of the region, although they tilt downward slightly toward the center. They reveal a distribution which appears to be very close to exponential in the vertical for much of the tank as shown by Figure 8. There is a cold boundary layer along the outside wall. Comparison of the sizes of the different regions to boundary layer length scales will be made in the discussion section.

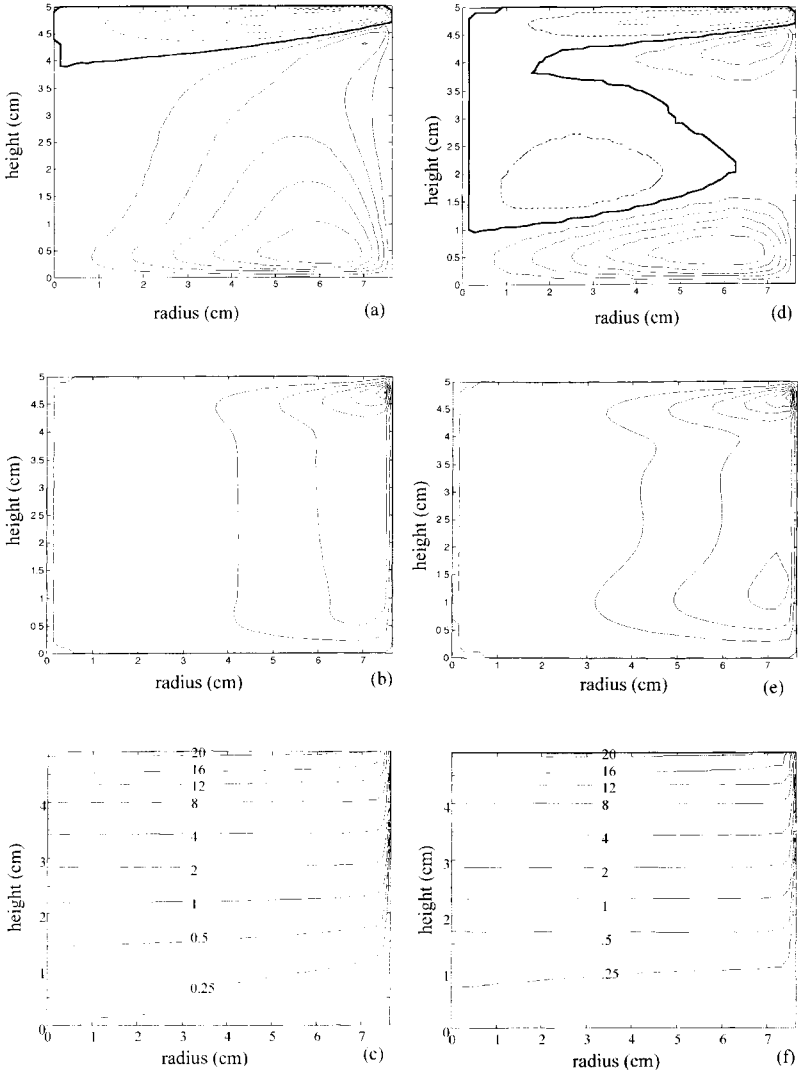

FIGURE 7 Flow and temperature from numerical calculations for two different rotation rates. (a), (d), Contours of azimuthal velocity. Values range from 0.05 cm/s downward with intervals of 0.01. The zero contour is darkened and negative values are dashed. (b), (e) Meridional streamfunction. Values start at 0 and range downward in intervals of 0.2 cm^2/s. (c), (f) Isotherms. Temperature given in °C. For (a) – (c), $f = 0.5\,s^{-1}$ and for (d) – (f), $f = 0.063\,s^{-1}$.

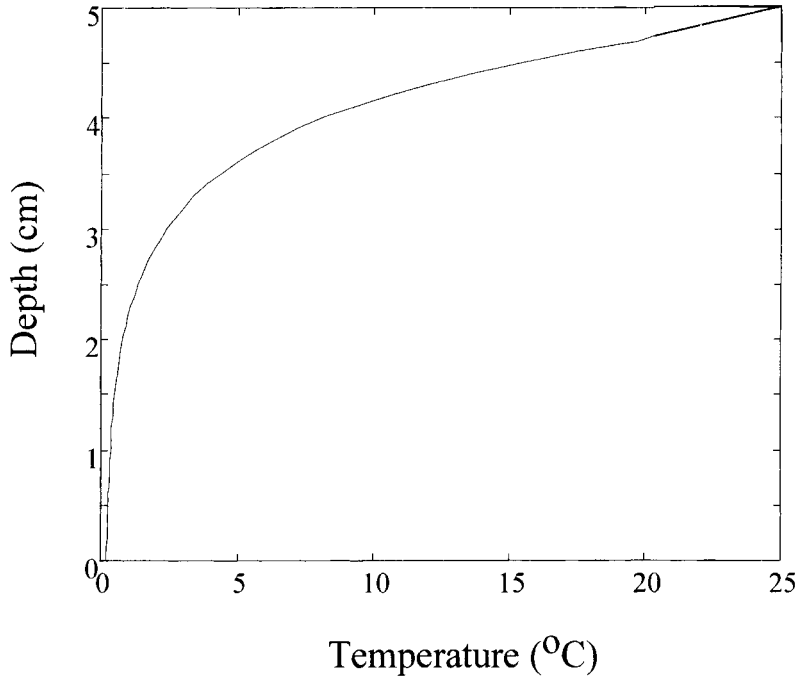

FIGURE 8 Vertical temperature profile at a typical middle radius (3 cm) for the temperature distribution shown in Figure 7c.

For the same eight parameter combinations as in the laboratory, numerical results (Fig. 9) show that maximum values of velocity increase with rotation rate but have little increase with temperature difference. The quantitative value of numerical velocity exceeds experimental results by order one factors. Possible causes of the discrepancy are mentioned in the discussion section.

One numerical run was carried out for the case of a free slip surface on the top of the basin. This corresponds more closely to a possible ocean situation in a case with small wind stress. Since the Ekman layer near the free surface is less effective at pumping water to the interior, one expects that the azimuthal velocity near the surface will be greater than with a rigid lid and possibly that anti-cyclonic circulation will penetrate to greater depths. Figure 10 illustrates the azimuthal velocity. The anti-cyclonic near-surface and cyclonic near-bottom circulation are obvious.

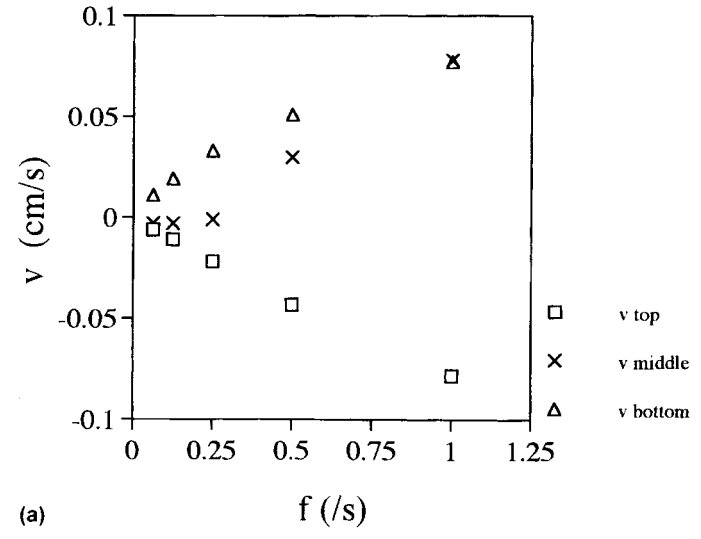

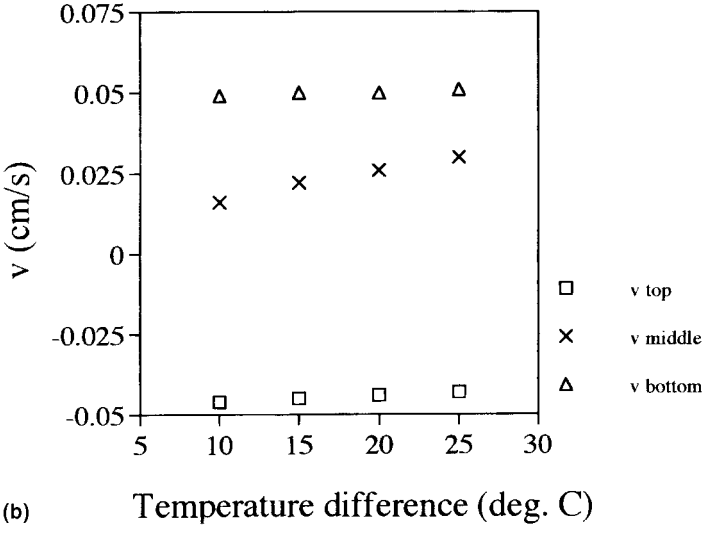

FIGURE 9 Maximum values of azimuthal velocity from numerical simulations. (a) Parameters correspond to those in the laboratory experiments shown in Figure 6a with fixed temperature and rotation rate varied. (b) Parameters correspond to those used in the laboratory experiments shown in Figure 6b with fixed rotation rate and varied temperature difference.

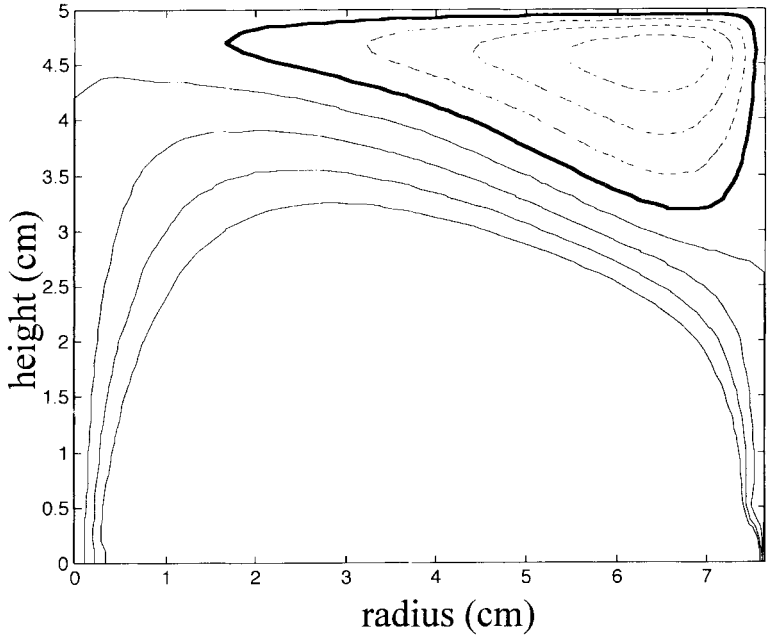

FIGURE 10 Distribution of azimuthal velocity for a case where the basin is heated from above with a free slip upper boundary condition. Maximum contour value is 0.04 cm/s and intervals are 0.01. The zero contour is darkened and negative values are dashed Experimental parameters are the same as those in Figures 7a–c.

3. SIDEWALL TEMPERATURE DRIVEN EXPERIMENTS

The next experiments had both heating and cooling imposed along the sidewall. Over ten sidewall temperature driven experiments were conducted. The apparatus is sketched in Figure 3b. The temperature differed between the upper and the lower halves of the sidewall of a cylindrical tank. This was intended to put energy into the lowest order baroclinic vertical mode. The tank was 37.5 cm diameter with water 25 cm deep. The top surface was subjected to as little stress as possible as a model of zero wind stress. A thin layer of air lay above the top surface and was shielded from the room with a tight lid. This lid was vital for two reasons. First, it eliminated drag from motionless room air, which of course has velocity different from the surface of rotating water. Second, it eliminated evaporation which would have significantly cooled the tank from above. A warm water bath fixed at 22°C

surrounded the upper half of the tank, and a second bath at colder temperature surrounded the lower half. The two baths were separated vertically by a horizontal layer of 2.5 cm thick Styrofoam. The two baths and the enclosed cylinder were contained in a square Plexiglas container on a turntable rotating at a 60 second period ($f = 0.21\ s^{-1}$).

To visualize the flow the thymol blue technique was used as before, but the brass rod electrodes were more complex. The active parts of the electrodes were 10 cm long. They were held horizontally by another vertical rod insulated electrically with lacquer. The vertical rod was located 2 cm from the sidewall. The electrodes were spaced above each other at intervals of 3 cm from the bottom of the cylinder tank to the top. The holding rod was positioned near the cylindrical wall and the electrodes were pointed radially inward, so when one sighted along the electrodes with them lying between the cylinder axis and the observer, dye coming off them indicated cyclonic circulation (positive velocity) to the right or anti-cyclonic circulation to the left. Images of the dye were recorded both photographically and on video tape.

One photograph of such dye streaks is shown in Figure 11. This flow possessed cyclonic flow near the top, anti-cyclonic flow at mid depth and a very small cyclonic flow just at the bottom. All flows in this experimental configuration possessed such a velocity distribution. The bottom cyclonic circulation was very weak in some examples, such as the example shown in the photograph, but in other runs the bottom cyclonic circulation was stronger. To obtain quantitative indication of the parameters that govern the circulation, a set of runs was conducted in which all parameters were kept the same except for temperature difference, which was systematically varied from 1 to 12°C.

As in the previous experiments the dye streak technique reveals a velocity profile so that it is easy to locate the levels of fastest flow. It was easy to measure an approximation to peak velocities at the top, middle and bottom. These were measured by taking data from videotape of dye position as a function of time. The tapes were recorded 4, 6, and 8 hours after the start. The results for the runs with assorted temperature differences are shown in Figure 12. Velocity so plotted is the maximum velocity of a dye streak. Although it would have been possible to impose a polynomial fit to the velocity data at the various depths and then take maxima from the polynomial, we opted to plot the actual data instead. The maxima should disagree

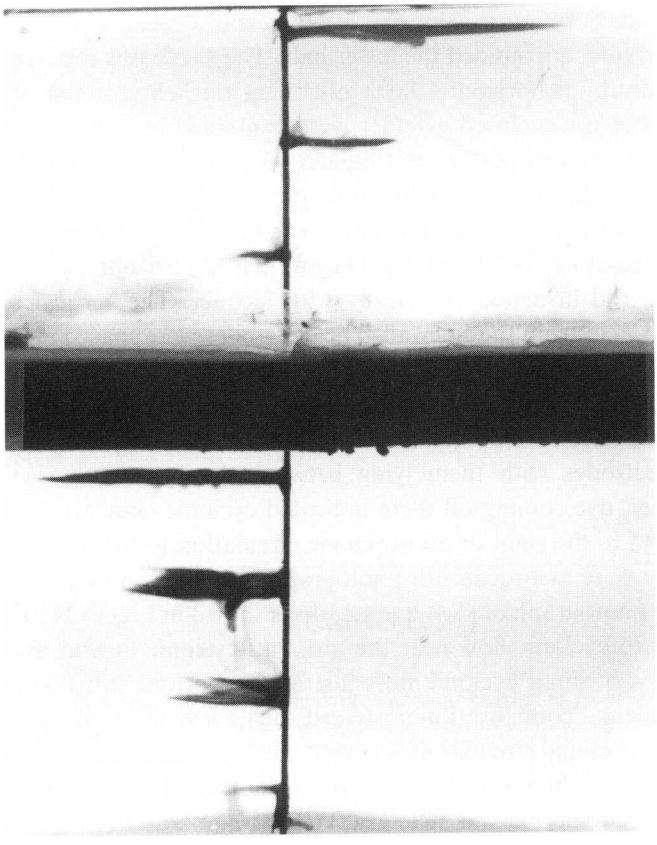

FIGURE 11 Photograph of dye streaks in the apparatus with a boundary temperature distribution as sketched in Figure 3b. Cyclonic flow direction is to the right. Insulation from the outer bath intersects the view at mid-depth.

with the data by tens of percent. In planning these experiments, emphasis was on the qualitative nature of these flows rather than precise quantitative fits, so this was thought sufficient. All velocities systematically increased with the increase in external temperature. Velocities of both signs were found in all observations. And finally, there was no evidence of non-axisymmetric flow.

The temperature profile was measured to see how the field compared with the linear conductive solution. Figure 13 shows an isotherm section taken by an array of thermistor probes that were lowered slowly through the tank after it had been spinning for over eight hours.

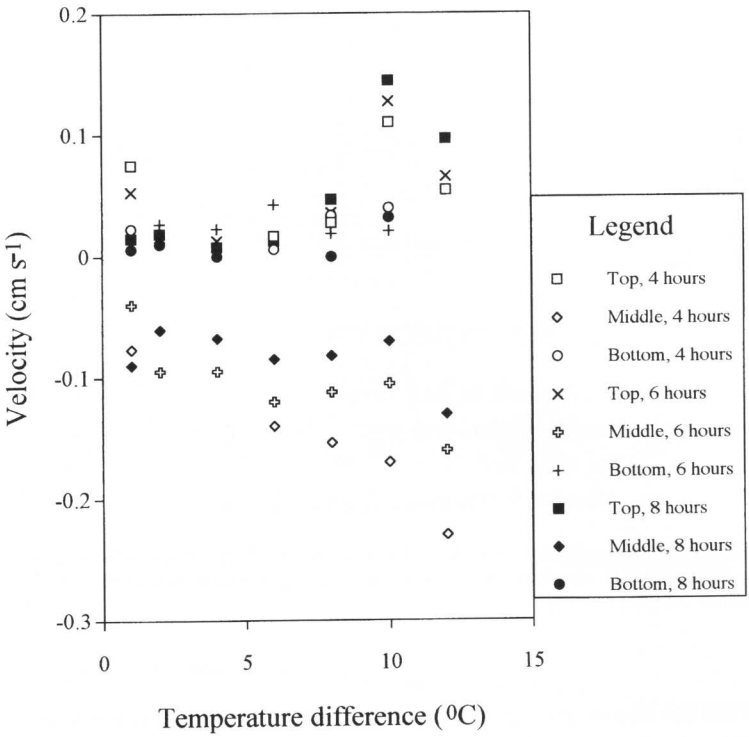

FIGURE 12 Velocity of the fastest speeds after 4, 6, and 8 hours.

The temperature field is not like the conductive solution, in which lateral temperature variation scales with vertical temperature variations. Instead there is strong vertical stratification with small lateral variations. Clearly the advection of heat is important to maintain this stratification, a result which was also found in the preceding numerical studies.

The dynamics of this experiment is similar to the dynamics of the first experiment. Imagine this experiment with a rigid lid on the surface. Let the temperature of upper and lower half of the sidewalls be $T_0 \pm \Delta T/2$ respectively, then the distribution of the azimuthal velocity is symmetric and the stream function and deviation of the temperature from average are anti-symmetric. Vertical velocity as well as vertical gradients of azimuthal and radial velocities are equal to zero

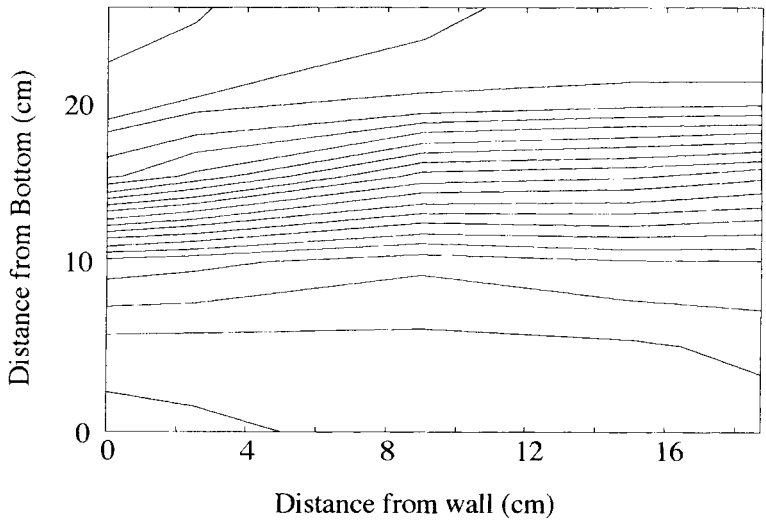

FIGURE 13 Temperature section across an experiment after more than eight hours. The fluid is stably stratified. A lateral temperature gradient is visible as a small tilt. Contour interval is 1°C.

on the middle of the basin due to the symmetry. Thus the circulation within the lower half of the basin is very similar to the free-slip circulation in the previous section (Fig. 10). Using symmetry to find the circulation in the top half, azimuthal circulation consists of two cyclonic jets near the surface and near the bottom. Anti-cyclonic circulation occupies the middle part of the basin. The secondary circulation in a vertical radial section consists of two cells of circulation: anti-clockwise in the upper half and clockwise in the lower part of the basin. Upwelling occupies the region near the heated half of the wall and downwelling occupies the region near the cooled half of the wall. The counteracting vertical motion in the interior of the basin leads to the formation of an inner thermocline around the depth where $w = 0$ as in the work of Stommel and Webster (1962). The inner thermocline is obvious in Figure 13.

Numerical simulations used the boundary conditions, at the top

$$\frac{\partial u}{\partial z} = \frac{\partial v}{\partial z} = w = \frac{\partial T}{\partial z} = 0 \quad \text{at } z = 0, \tag{9}$$

at the bottom

$$u = v = w = \frac{\partial T}{\partial z} = 0 \quad \text{at } z = H, \tag{10}$$

and at the center and outer wall

$$u = v = \frac{\partial T}{\partial r} = 0 \quad \text{at } r = 0, \tag{11}$$

$$u = v = 0 \quad \text{at } T = T_b(z),\ r = R, \tag{12}$$

where $T_b(z) = \Delta T/2$ along the upper half of the wall and minus that amount along the bottom half. The spinup time was from 5 to 7 hours, and results are only shown after the tank had fully come to steady state. Figure 14 shows contours of azimuthal velocity, meriodonal

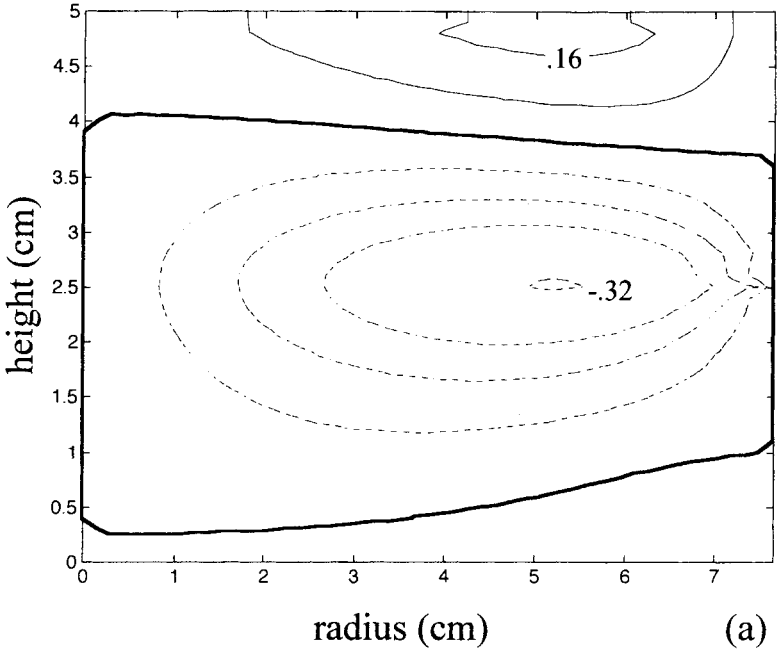

FIGURE 14 (a) Distribution of the azimuthal velocity when the heating and cooling are both from the side wall. External temperature difference is 12°C and contours are every 0.08 cm/s. (b) The meridional streamfunction. (c) The temperature distribution. Note the similarity with Figure 13.

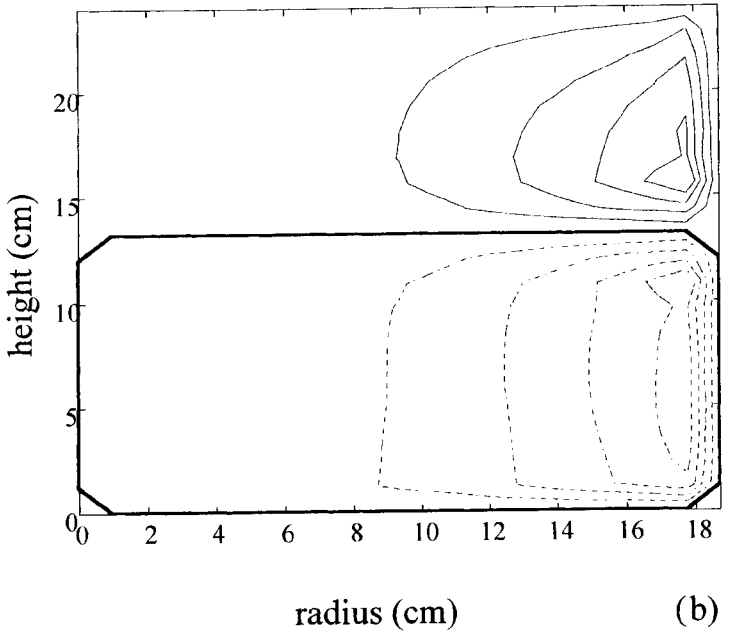

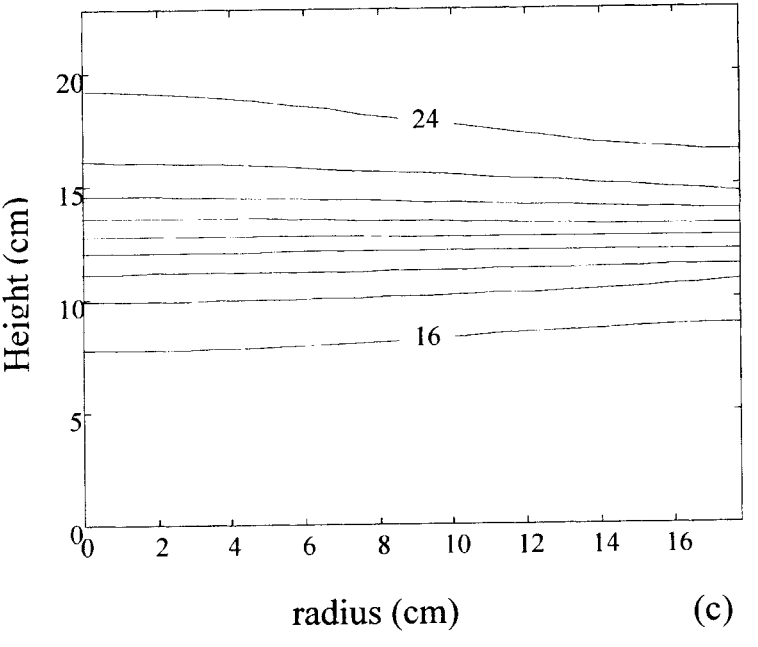

FIGURE 14 (Continued).

circulation and isotherms for one set of calculations with the same parameters as the laboratory and $\Delta T_v = 10°C$. The azimuthal circulation has three-layers and secondary circulation consists of two cells. The temperature distribution has many features seen in the laboratory profile, such as the strong inner thermocline which forms in the middle of the basin. The horizontal gradients of temperature are significantly less than the vertical gradients within the thermocline.

The values of velocity maxima at the three levels were measured for numerical runs conducted for eight hours. The values are shown in Table I. They will be compared with the experimental values and with a proposed velocity scale in the discussion.

4. DISCUSSION

Both the laboratory experiments and numerical simulations show important general features which we expect could be typical of steady buoyancy driven currents in a uniformly rotating basin. The azimuthal circulation has a layered structure in the vertical direction. The number of cyclonic and anti-cyclonic maxima depends on the distribution of heating and cooling along the boundary of the basin and on the type of dynamic boundary conditions on the surface of the basin. In all cases at least one cyclonic flow and one anti-cyclonic flow existed and in some experiments there was cyclonic flow at the bottom and top with anti-cyclonic circulation in the middle. In the case with a temperature imposed along the sidewall an internal thermocline was seen. This implies there are two meridional cells lying over each other with opposite signs of rotation. No deviation from axisymmetry was seen in any experiment.

The lack of precise quantitative agreement between the numerical results and experiment is not surprising. The experiments were

TABLE I Top, middle, and bottom velocities after 8 hours at a distance of 2 cm from the outer wall for different values of temperature difference. These data will be shown in Figure 15

Temperature difference	1	2	4	6	8	10	12
Velocity top	0.077	0.096	0.122	0.141	0.158	0.178	0.192
middle	0.102	−0.129	−0.156	−0.174	−0.190	−0.204	−0.214
bottom	0.016	0.019	0.022	0.024	0.027	0.031	0.031

designed long before the numerical runs were contemplated. The objective was to reveal qualitative aspects of the flow and to reveal some of the scaling tendencies. The glass sidewalls do not possess exactly constant temperature. In the first configuration there are rounded corners in the beakers. There may also be some leakage of heat between the walls of the two beakers above the gasket holding the top cyclinder. In addition, the relatively large electrodes may clearly exert some additional drag and conduct some heat away. And finally the free-slip boundary condition for the second experimental configuration may have some unknown drag from surfactants.

The nonlinear (heat convection) terms in Eq. (4d) are obviously large in the laboratory experiments. Strictly speaking such terms should be retained in the dynamical components of Eqs. (4a) and (4b) and not just in the temperature equation. This must cause some error as does the neglect of friction from vertical velocity in (4c).

Undoubtedly some of the boundary layers are small enough to be poorly resolved in the numerical model. Linearized studies show there are three important dimensionless numbers (Barcilon and Pedlosky, 1967a) Ekman number $E = 2\nu/fH^2$, Prandtl number $\sigma = \nu/\kappa$ and stratification $S = g\alpha\Delta T_v/f^2H = N^2/f^2$. The parameter N is the Brunt-Vaisala frequency and ΔT_v is a vertical temperature change which produces ambient stratification. Temperature gradient will be assumed to be constant in order to fix boundary layer sizes. There are three boundary layers for small E of size $H\sqrt{E/2}$, $R/\sqrt{\sigma S}$, and $H(E/2)^{1/3}$. The first is the well-known Ekman layer. The second has no formal name although it has been studied by Barcilon and Pedlosky (1967) and Pedlosky *et al.* (1997). The third is a frictional sidewall boundary layer.

Estimates of their sizes compared to the numerical grid size show that some boundary layers are too small to be precisely resolved numerically. For both laboratory and numerical experiments, E takes the smallest value of 0.0008 for $f = 1$ and the largest of 0.0128, for $f = 0.063$ so the first (Ekman) boundary layer thickness ranged from 0.1 to 0.4 cm thick. The numerical grid was 51×51 and depth of the cylinder was 5 cm, so each grid is approximately 0.1 cm in vertical size. Therefore, Ekman layers are of order of the grid size and thus are not well resolved for any rotation rate. Pedlosky *et al.* (1997) show that for $\sigma S \ll 2\sqrt{E}$ the Ekman layers are important but that for $\sigma S \gg 2\sqrt{E}$

they are less important factors in the dynamics, so the numerical results for large stratification may be superior to those with small stratification. The second boundary layer thickness ranges from 4.57 to 0.29 cm for a ten degree vertical temperature scale (for f largest to smallest, respectively). For a one degree vertical temperature scale the thickness ranges from 45.7 to 2.9 cm. This boundary layer was discussed by Pedlosky *et al.* (1997). It represents a balance between vertical and lateral (secondary, or meriodonal) circulation. In the cases where it is larger than fluid depth, fluid can move vertically throughout the interior. When this boundary layer is some fraction of the fluid depth, vertical interior motion is only possible within this boundary layer. This boundary has thickness greater than the numerical grid spacing, so it should be thick enough to be well resolved in almost all of the numerical runs.

The third sidewall boundary layer is not found in the solutions of Pedlosky *et al.* (1997) since sidewall boundary layers were shown to be inactive because of zero lateral heat flux in that problem. But it is found in nonstratified fluid, and thus is well known. It permits vertical flow near the sides of the channel and does not depend on the value of stratification. Its thickness ranges from 0.36 cm to 0.93 cm. It is probably reasonably well resolved in the numerical model.

Strongly non-linear dynamics is reproduced in the laboratory and numerical runs due to the advection of heat. Let us define the thermal Rossby number as

$$R_o = \frac{V}{fH} = \frac{g\alpha\Delta T}{f^2 H},$$

where the velocity scale is

$$V = \frac{g\alpha\Delta T}{f} \tag{13}$$

from linear theory. We find that thermal Rossby number is of the order of unity or higher in nature. However the calculated and measured velocities in the preceding sections have significantly smaller magnitude than the linear velocity scale ($8\,\mathrm{cm\,s^{-1}}$ for $f = 0.25\,\mathrm{s^{-1}}$ and

$\Delta T = 10°C$) used above. We can correct the scale of velocity bearing in mind that the thickness of thermocline D_b is significantly less than the depth of the basin. Then the scale of the pressure is $g\alpha\Delta T D_b$ from the hydrostatic equation and the geostrophic relation gives $v_e \propto (g\alpha\Delta T D_b/fR)$ where R is the radius of the basin. The scale of the vertical velocity is defined from the divergence within the Ekman layer $w_e \propto v_e\sqrt{2(\nu/fR^2)}$. Another estimate of the vertical velocity may be found from the balance between vertical thermal conduction and vertical advection of heat so that $w_e \propto \kappa/D_b$. Equating the two estimates and using v_e, we obtain

$$D_b \propto R\sqrt{\frac{f^2}{2g\alpha\Delta T P_r}\left(\frac{2\nu}{f}\right)^{1/2}} \propto E^{1/4}(2P_r R_0)^{-1/2}R, \tag{14}$$

which leads to a velocity scale

$$v_e \propto \sqrt{\frac{g\alpha\Delta T}{2\sigma}\left(\frac{2\nu}{f}\right)^{1/2}}. \tag{15}$$

An energy argument also produces this velocity scale. Let us equate the energy released by buoyancy with the energy dissipated by friction in the Ekman layers. The energy per unit surface area released by buoyancy (normalized by density) is

$$E_b = g\int_0^H \frac{w\rho'}{\rho_0}dz = g\int_0^H w\alpha T' dz, \tag{16}$$

$$E_b = \frac{g\alpha\dot{H}H}{\rho_0 C_p}, \tag{17}$$

where $\dot{H}$, ρ', C_p are heat flux, density deviation from the horizontally averaged density ρ_0, and specific heat, respectively. To get (17), it is assumed that heat flux per unit area $\dot{H} = \rho_0 C_p \overline{wT'}$ (overbar denotes horizontal average) is relatively constant within the thermocline. Since the temperature field is in steady state, downward conduction of heat by diffusion in this temperature gradient must be balanced by upward advection. Setting the advective heat flow to the magnitude of

conductive heat flow

$$\dot{H} = \rho C_p \overline{wT'} \propto k \frac{\Delta T}{H}, \tag{18}$$

where k is thermal conductivity, (17) becomes

$$E_b \propto \frac{g\alpha k \Delta T}{\rho_0 C_p} = g\alpha\kappa\Delta T. \tag{19}$$

This diffusively driven liberation of potential energy must be balanced by frictional dissipation F_{dis}. This happens either in the interior or, more likely, in the bottom Ekman layer where

$$F_{\text{dis}} \propto \frac{\tau v_e}{\rho_0} \propto \frac{\nu v_e^2}{\delta} \tag{20}$$

and $\delta = \sqrt{2\nu/f}$ is Ekman layer thickness. Equating dissipation with buoyancy energy release [*e.g.* (19) and (20) with the definition of Ekman layer thickness] produces a formula for v_e which differs from (15) only by the factor $1/\sqrt{2}$.

The linear velocity scale (13) and nonlinear scale (15) are included as two straight lines and two curves, respectively in Figure 15, which also contains velocity measurements from both the numerical (Tab. I) and laboratory experiments of the second configuration. There is crude agreement with some of the magnitudes of the nonlinear velocity scale with both cyclonic and anti-cyclonic flow from numerical simulations. In other cases, the agreement is poor, for example there is poor agreement between the velocity scale and both the cyclonic velocity maxima near the top and bottom of the laboratory experiments, and the cyclonic velocity at the bottom of the numerical tank. The surface cyclonic flow is greater in numerical simulations than in laboratory experiments except for two of the experimental points in Figure 15. Since the value of cyclonic surface flow in the laboratory is clsoe to the value of cyclonic bottom flow, the shielding of the basin from the surface wind stress probably did not ensure zero surface stress. It is well known that surface tension provides partial rigidity to weak shear flows. Although it is clear that some of the velocity fields have similar magnitudes to the nonlinear velocity scale, this comparison only shows

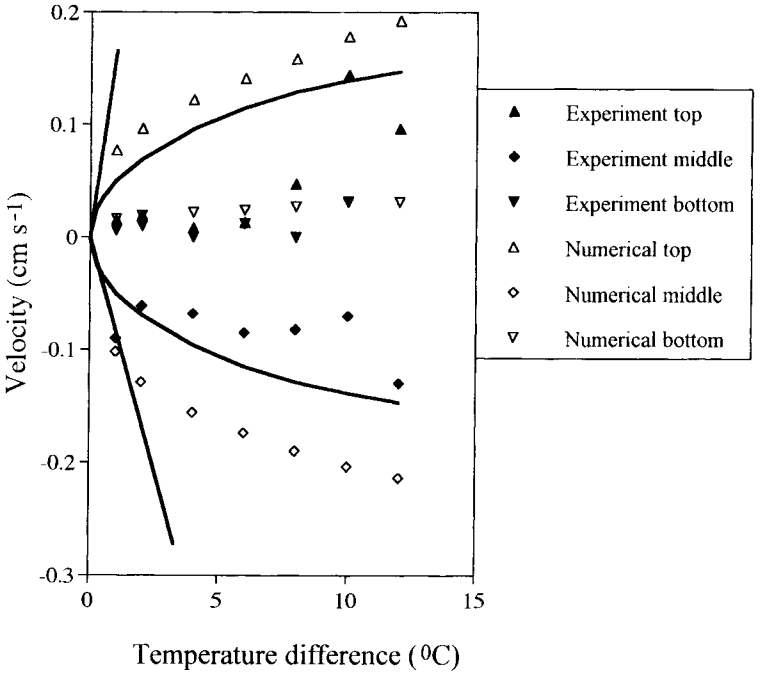

FIGURE 15 Comparison of velocity scales [straight lines – Eq. (13), curves – Eq. (15)] with laboratory and numerical data.

that some velocities have about the same magnitude. It is only meant to be suggestive at best.

The experiments were principally designed to reveal qualitative details of the flow. The relatively small containers in the first configuration were made of poorly conducting materials with rounded walls. Also there was some possible heat loss, plus the electrodes add some extra drag and thermal conduction not in theory. Thus it is not surprising that the results of the first configuration do not compare quantitatively with numerical results or scalings. Equation (15) overestimates velocities in the thermocline driven numerical experiments by more than a factor of two, which in turn are greater than the laboratory results by about a factor of two. In contrast to the numerical runs with side heating, velocity is not seen to be sensitive to temperature difference in Figure 6. Velocity may be proportional to f to some positive power although the scatter is great. It cannot be

determined whether this significantly differs from the scaling from the thermal boundary layer analyses or energy argument, where velocity is proportional to $f^{-1/4}$.

One could use formulae (14), (15) to find an anticipated velocity and pycnocline scales for buoyancy driving. Consider Black Sea conditions with temperature difference of 16°C which corresponds to the difference of 4 ppt in salinity between the surface and deep waters of the Black Sea. The depth of the Black Sea is 2 km. The horizontal size of the deep part of the Black Sea is about 200 km along the meridian and 1000 km in the zonal direction. A round basin with the same area of the surface has the radius $R = 250$ km. Take (14) and (15) and use coefficient of expansion 2×10^{-4}, Prandtl number = 10, vertical viscosity of 1 $cm^2 s^{-1}$, radius of the basin $R = 250$ km and $f = 10^{-4} s^{-1}$. This gives the thickness of the pycnocline of 40 m and the velocity scale 5 $cm\,s^{-1}$ which is reasonably consistent with the real parameters of the Black Sea.

In both experiments sidewall cooling induces downwelling within a thin boundary layer near the outer wall. The deep interior of the basin at the same level is thus occupied by upwelling which supports a thermocline. Accordingly, we might anticipate the presence of deep interior upwelling in assorted marginal seas. In the Black Sea basin the observed distribution of the salinity in the surface layers (Bulgakov and Korotaev, 1987; Bulgakov, 1987) is consistent with upwelling whose value determines the age of deep waters of the Black Sea.

Direct observations (Bulgakov *et al.*, 1994; Bulgakov and Kushnir, 1996) are consistent with both cyclonic and anti-cyclonic circulation in the upper regions of the Black Sea but they are contaminated by the wind-influenced surface gyre. There is not much evidence for geostrophic flow of a bottom cyclonic gyre in deep marginal seas. Additional measurements of the distribution of circulation of deep basins (deep ocean trenches, Panama Basin, Philippine Basin), marginal seas (Caribbean, Indonesian basins, Mediterranean, Black Sea, Arctic Ocean, Baltic), and deep lakes (Baikal, Great Lakes), may reveal circulation layers like those in the theory and experiments. In other cases, they may be overridden by processes akin to Stommel-Arnos circulation, or to the JEBAR eddy flux processes found by Spall (1994). If two signs of circulation are present, documentation of deep circulation would help to quantify the maguitude of bottom drag, the

manner by which the buoyancy, momentum and vorticity is transported by the fluid, and the distribution of buoyancy flux at the boundaries. These processes remain poorly understood in nature and may be clarified with studies of circulation in small deep basins.

Acknowledgments

Travel for initial phases of this work was provided by Dr. Craig Dorman under the Director's discretionary funds of the Woods Hole Oceanographic Institution. R. Frazel assisted with the experiments. Support for the thermal experiments was provided by the Office of Naval Research, Coastal Sciences section under Grant No. N00014-89-J-1037. Suggestions by K. Helfrich and J. Toole at various stages of this work are gratefully acknowledged. Contribution Number 8598 of the Woods Hole Oceanographic Institution.

References

Aagaard, K., "On the deep circulation in the Arctic Ocean," *Deep Sea Res.* **28A**, 251–68 (1981).

Aubrey, D. G., Oguz, T., Demirev, E., Ivanov, V., McSherry, T., Daiconu, V. and Nikolaenko, E., Hydroblack 91, "Report of the CTD Intercalibration Workshop," *Woods Hole Oceanographic Institution Technical Report* **WHOI-92-10**, CRC-92-01 (1992).

Barcilon, V. and Pedlosky, J., "Linear theory of rotating stratified fluid motions," *J. Fluid Mech.* **29**, 1–16 (1967a).

Barcilon, V. and Pedlosky, J., "A unified linear theory of homogeneous and stratified rotating fluids," *J. Fluid Mech.* **29**, 609–21 (1967b).

Barcilon, V. and Pedlosky, J., "On the steady motions produced by a stable stratification in a rapidly rotating fluid," *J. Fluid Mech.* **29**, 673–90 (1967c).

Bennett, J. R., "Another explanation of the cyclonic circulation of large lakes," *Limnol. Oceanogr.* **20**, 108–110 (1975).

Bulgakov, S. N., "Investigation of the haline factors role in the Black Sea circulation and water structure formation," *Ph.D. Thesis*, p. 155 Marine Hydrophysical Institute, Sevastopol, USSR (1987).

Bulgakov, S. N. and Korotaev, G. K., "Analytical model of the jet stream circulation in semi-enclosed seas," *Marine Hydrophys. Journal* pp. 18–24 (1987).

Bulgakov, S. N. and Kushnir, V. M., "Vertical structure of the current field in the Northern Black Sea," *Oceanol. Acta* **19**, 513–522 (1996).

Bulgakov, S. N., Demyshev, S. G. and Korotaev, G. K., "Modelling of the Black Sea circulation and water stratification," *Report of "Black Sea Problems" Meeting, Sevastopol*, 10–17 November, pp. 34–53 (1992).

Bulgakov, S. N., Ivanov, V. A. and Korotaev, G. K., "Unknown countercurrent in the Black Sea", Reports of Ukrainian Ac. Sci. Kiev, *Naukova Dumka* **12**, 110–114 (1994).

Bulgakov, S. N., Korotaev, G. K. and Whitehead, J. A., "The role of the buoyancy fluxes in the formation of a large-scale circulation and stratification of sea-water Part 1: The Theory," *Izvestiya-Atmospheric and Oceanic Physics* **32**, 548–556 (1996a).

Bulgakov, S. N., Korotaev, G. K. and Whitehead, J. A., "The role of the buoyancy fluxes in the formation of a large-scale circulation and stratification of sea-water Part 2: Laboratory Experiments," *Izvestiya-Atmospheric and Oceanic Physics* **32**, 506–513 (1996b).

Chao, S. L. and Boicourt, W., "Onset of estuarine plume," *J. Phys. Oceanogr.* **16**, 2137–2149 (1986).

Csanady, G. T., "Mean circulation in shallow seas," *J. Geophys. Res.* **81**, 5389–99 (1976).

Csanady, G. T., "On the cyclonic mean circulation of large lakes," *Proc. Nat. Acad. Sci.* **74**, 2204–2208 (1977).

Emery, K. O. and Csanady, G. T., "Surface Circulation of lakes and nearly land-locked seas," *Proc. Natl. Acad. Sci. USA* **70**, 93–97 (1973).

Gill, A. E., "Adjustment under gravity in a rotating channel," *J. Fluid Mech.* **77**, 603–621 (1976).

Griffiths, R. W., "Gravity Currents in Rotating Systems," *Annu. Rev. Fluid Mech.* **18**, 59–89 (1986).

Griffiths, R. W. and Hopfinger, E. J., "Gravity currents moving along a lateral boundary in a rotating fluid," *J. Fluid Mech.* **134**, 357–399 (1983).

Johnson, Gregory C., "Deep water properties, velocities, and dynamics over ocean trenches," *J. Mar. Res.* **56**, 329–347 (1998).

Monismith, S. G. and Maxworthy, T., "Selective withdrawal and spin-up of a rotating stratified fluid," *J. Fluid. Mech.* **199**, 377–401 (1989).

Oguz, T., Malanotte-Rizzoli, P. and Aubrey, D., "Wind and thermohaline circulation of the Black Sea driven by yearly mean climatological forcing," *J. Geophys. Res.* **100**, C4, 6845–6863 (1995).

Pedlosky, J., Whitehead, J. A. and Veitch, G., "Thermally driven motions in a rotating stratified fluid: theory and experiment," *J. Fluid Mech.* **339**, 391–411 (1997).

Spall, M. A., "Wave-induced abyssal recirculations," *J. Mar. Res.* **52**, 1051–1080 (1994).

Stern, M. E., "Geostrophic fronts, bores, breaking and blocking waves," *J. Fluid Mech.* **99**, 687–704 (1980).

Stern Melvin, E., Whitehead, J. A. and Hua, B. L., "The intrusion of a density current along the coast of a rotating fluid," *J. Fluid Mech.* **123**, 237–265 (1982).

Stommel, H. and Arons, A. B., "On the abyssal circulation of the World Ocean-I. Stationary Planetary flow patterns on a sphere," "II. An idealized model of the circulation pattern and amplitude in oceanic basins," *Deep Sea Res.* **6**, 140–154, 217–233 (1960).

Stommel, H. and Webster, J., "Some properties of Thermocline Equations in a Subtropical gyre," *J. Mar. Res.* **20**, 42–56 (1962).

Takano, K., "A complimentary note on the diffusion of the seaward river flow off the mouth," *J. Oceanogr. Soc. Japan* **11**, 1–3 (1955).

Trukhchev, D. I. and Demin, Y. L., *Woods Hole Oceanographic Institution Technical Report* **WHOI-92-34**, CRC-92-02 (1992).

Wang, D. P., "The strait surface outflow," *J. Geophys. Res.* **92**, 10807–10825 (1987).

Warren, B. A., "Deep circulation of the World Ocean," In: *Evolution of physical oceanography* (Eds., Warren, B. A. and Wunsch, C.), pp. 6–41 Cambridge MA: MIT Press (1981).

Whitehead, J. A. and Chapman, D. C., "Laboratory observations of a gravity current on a sloping bottom: the generation of shelf waves," *J. Fluid Mech.* **172**, 373–399 (1986).

Whitehead, J. A. Jr. and Miller, A. R., "Laboratory simulation of the gyre in the Alboran Sea," *J. Geophys. Res.* **84**, C7, 3733–3742 (1979).

Wunsch, C., "On mean drift in large lakes," *Limnol. Oceanogr.* **18**, 793–795 (1973).